Zn^{2+}-Chelating Motif-Tethered Short-Chain Fatty Acids as a Novel Class of Histone Deacetylase Inhibitors

Qiang Lu,[†] Ya-Ting Yang,[†] Chang-Shi Chen,[†] Melanie Davis,[‡] John C. Byrd,[‡] Mark R. Etherton,[§] Asad Umar,[§] and Ching-Shih Chen*[,†]

Division of Medicinal Chemistry and Pharmacognosy, College of Pharmacy, and Division of Hematology-Oncology, The Arthur James Comprehensive Cancer Center, The Ohio State University, Columbus, Ohio 43210, and Laboratory of Biosystems & Cancer, Center for Cancer Research, National Cancer Institute, Bethesda, Maryland 20892

Received July 31, 2003

Among various classes of histone deacetylase (HDAC) inhibitors, short-chain fatty acids exhibit the least potency, with IC_{50} in the millimolar range. We rationalized that this weak potency was, in part, attributable to their inability to access the zinc cation in the HDAC active-site pocket, which is pivotal to the deacetylation catalysis. We thus explored the structural optimization of valproate, butyrate, phenylacetate, and phenylbutyrate by coupling them with Zn^{2+}-chelating motifs (hydroxamic acid and *o*-phenylenediamine) through aromatic *ω*-amino acid linkers. This strategy has led to a novel class of Zn^{2+}-chelating, motif-tethered, short-chain fatty acids that exhibited varying degrees of HDAC inhibitory potency. One hydroxamate-tethered phenylbutyrate compound, *N*-hydroxy-4-(4-phenylbutyrylamino)benzamide (HTPB), displayed nanomolar potency in inhibiting HDAC activity. Exposure of several cancer cell lines to HTPB at the submicromolar level showed reduced cell proliferation accompanied by histone hyperacetylation and elevated $p21^{WAF/CIP1}$ expression, which are hallmark features associated with intracellular HDAC inhibition.

Introduction

The acetylation status of core histones plays a pivotal role in regulating gene transcription through the modulation of nucleosomal packaging of DNA.[1−3] In a hypoacetylated state, nucleosomes are tightly compacted, resulting in transcriptional repression due to restricted access of transcriptional factors to their targeted DNA. Conversely, histone acetylation leads to relaxed nucleosomal structures, giving rise to a transcriptionally permissive chromatin state. The level of this posttranslational modification is maintained by a dynamic balance between the activities of histone acetyltransferases (HATs) and histone deacetylases (HDACs), both of which are recruited to target genes in complexes with sequence-specific transcription activators. Aberrant regulation of this epigenetic marking system has been shown to cause inappropriate gene expression, a key event in the pathogenesis of many forms of cancer.[4−6] Moreover, evidence demonstrates that inhibition of HDAC triggers growth arrest, differentiation, and/or apoptosis in many types of tumor cells by reactivating the transcription of a small number of genes.[7−11] These in vitro findings have also been confirmed in xenograft models, suggesting that modulation of HDAC's function might be targeted for the prevention and/or therapeutic intervention of cancer.

To date, several structurally distinct classes of HDAC inhibitors have been reported,[7−11] including short-chain fatty acids (e.g., butyrate, valproate, phenylacetate, and phenylbutyrate),[12−15] benzamide derivatives (e.g., MS-27-275),[16,17] trichostatin A (TSA) and analogues,[18−20] hybrid polar compounds [e.g., suberoylanilide hydroxamic acid (SAHA)],[21,22] cyclic tetrapeptides (e.g., apicidin),[23−26] and the depsipeptide FR901228.[26] Among these agents, short-chain fatty acids are the least potent inhibitors with IC_{50} in the millimolar range, as compared to micromolar or even nanomolar for other types of HDAC inhibitors. Although the use of short-chain fatty acids in cancer treatment has been reported, their therapeutic efficacy has been limited by low antiproliferative activity, rapid metabolism, and nonspecific mode of action.

Recently, X-ray crystallographic analysis of HDLP (histone deacetylase-like protein), a bacterial HDAC homologue, has revealed a distinctive mode of protein−ligand interactions whereby TSA and SAHA mediate enzyme inhibition.[27] The HDAC catalytic domain consists of a narrow, tubelike pocket spanning the length equivalent to four- to six-carbon straight chains. A Zn^{2+} cation is positioned near the bottom of this enzyme pocket, which, in cooperation with two His-Asp charge-relay systems, facilitates the deacetylation catalysis. Accordingly, the structures of TSA and SAHA might be divided into three motifs, each of which interacts with a discrete region of the enzyme pocket. These include a Zn^{2+}-chelating function (i.e., hydroxamic acid), an aliphatic chain as linker, and a polar, planar cap group (i.e., dimethylaminophenyl and phenylamino functions, respectively).[27] To mediate the enzyme inhibition, the long aliphatic chain facilitates the insertion of the HDAC inhibitor into the tubelike enzyme pocket, permitting the hydroxamate group to reach the polar bottom of the pocket and coordinate with the Zn^{2+}

* To whom correspondence should be addressed. Address: Parks Hall, Rm 336, 500 West 12th Avenue, The Ohio State University, Columbus, OH 43210-1291. Tel: (614) 688-4008. Fax: (614) 688-8556. E-mail: chen.844@osu.edu.

[†] Division of Medicinal Chemistry and Pharmacognosy, The Ohio State University.

[‡] Division of Hematology-Oncology, The Ohio State University.

[§] National Cancer Institute.

10.1021/jm0303655 CCC: $27.50
Published on Web 12/11/2003

cation. Meanwhile, the polar cap group at the other end of the spacer makes contacts at the pocket entrance, thereby capping the pocket. This unique mode of mechanism also applies to other potent HDAC inhibitors, while the structures of individual motifs vary. This three-component concept has proven successful in developing structural analogues of TSA and trapoxin as potent HDAC inhibitors.[19,28]

In light of this working model, we rationalized that the weak potency of short-chain fatty acids in HDAC inhibition was, in part, attributable to their inability to access the Zn^{2+} cation in the active-site pocket, which plays a pivotal role in the deacetylation catalysis. In the present study, we explored the structural optimization of short-chain fatty acids by tethering them with a Zn^{2+}-chelating motif via an aromatic linker. This strategy has led to the development of a novel class of Zn^{2+}-chealting, motif-tethered, short-chain fatty acids, some of which show inhibition of HDAC activity and cancer cell proliferation in nanomolar range, a 3 orders of magnitude improvement over their parent compounds.

Chemistry

In general, short-chain fatty acids exhibit HDAC inhibitory and antiproliferative activities in the millimolar range irrespective of the structure of the acyl chains.[8−10] Here, we propose that these fatty acids exerted HDAC inhibition through nonspecific hydrophobic interactions with surface residues located at the enzyme pocket entrance and/or the hydrophobic region inside the tubelike pocket. Accordingly, we examined the working hypothesis that the HDAC inhibitory potency of these short-chain fatty acids might be enhanced by tethering to a Zn^{2+}-chelating moiety through a hydrophobic spacer. In this study, we used two types of Zn^{2+}-chealting motifs that could reversibly coordinate with the zinc cation, i.e., hydroxamic acid and *o*-phenylenediamine. With regard to the spacer, we chose aromatic linkers in lieu of aliphatic chains for two reasons: (1) to enhance the structural rigidity of the conjugate and (2) to increase van der Waals contacts with the tubelike hydrophobic region of the pocket to improve binding affinity. The linkers used here included 4-(aminomethyl)benzoic acid, 4-aminobenzoic acid, (4-aminophenyl)acetic acid, 3-(4-aminophenyl)propionic acid, and 3-(4-aminophenyl)acrylic acid. Among them, 4-(aminomethyl)benzoic acid has been used as the linker for MS-27-275.[17] These aromatic ω-amino acids exhibited lengths equivalent to that of four- to six-carbon straight chains, in line with the depth of the hydrophobic region. For the first series of structural modifications, we employed valproic acid as lead to synthesize Zn^{2+}-tethered conjugates (Figure 1) according to the procedures depicted in Scheme 1 (A, compounds **1**−**8**; B, compounds **9** and **10**). For compounds **1**−**8**, valproic acid was coupled with four different ω-amino acid methyl ester spacers via EDC activation. The resulting esters were cleaved to acids via alkaline hydrolysis. Under typical peptide coupling conditions (BOPCl or EDC), the resulting acids were treated with Bn-protected hydroxylamine and Cbz-protected *o*-phenylenediamine to form, after hydrogenolysis, the respective anilides and hydroxamic acids (Scheme 1A). Compounds **9** and **10** were synthesized by direct coupling of 3-[4-(2-propylpentanoyl)phenyl]acrylic acid with *o*-phenylenediamine and hydroxylamine, respectively, under typical EDC coupling condition (Scheme 1B).

Results

Zn^{2+}-Chelating, Motif-Tethered Valproate Derivatives. The divergent conjugation of valproic acid with five different aromatic linkers and subsequently two Zn^{2+}-binding motifs yielded compounds **1**−**10**. These tethered conjugates displayed varying degree of HDAC inhibitory potency (Figure 2), with IC_{50} values ranging from 5 μM (compound **8**) to 80 μM (compound **5**). This potency was a 5−80-fold improvement over that of the parent molecule (IC_{50}, 0.4 mM). Moreover, removal of the valproyl moiety or the Zn^{2+}-chelating motif from any of these conjugates would completely abolish the HDAC inhibitory activity (data not shown), indicating the importance of the acyl function and the Zn^{2+}-chelating motif in the protein−ligand interactions. These data bore out our tethering strategy with short-chain fatty acids as molecular platforms to develop a new class of HDAC inhibitors.

Among the 10 tethered conjugates examined, compounds **1**, **2**, **4**, and **8** represented the optimal derivatives (IC_{50}, 5−8 μM), followed by **3**, **9**, and **10** (IC_{50}, 10−20 μM). Relatively, the hydroxamates (compounds **2**, **4**, **6**, **8**, and **10**) were generally more potent than their phenylenediamine counterparts (compounds **1**, **3**, **5**, **7**, and **9**). Moreover, the aromatic linker exhibited a subtle effect on HDAC inhibitory activity. Among the five aromatic ω-amino acids examined, (4-aminophenyl)-acetate gave rise to conjugates with the least HDAC inhibitory potency (**5** and **6**), while 4-(aminomethyl)-benzoate appeared to be optimal. For further structural modifications, compounds **1**, **2**, **4**, and **8** were used as leads, since all of them exhibited $IC_{50} < 10$ μM.

Structural Optimization. The finding that removal of the valproyl group would completely abrogate the inhibitory activity of the conjugate underscored the importance of the acyl moiety in interacting with the active-site pocket. We further examined the stereoelectronic effect of substituting the valproyl group in compounds **1**, **2**, **4**, and **8** with a butyryl, phenylacetyl, or phenylbutyryl function on HDAC inhibition (Figure 3). All these derivatives showed an improved potency in HDAC inhibition as compared to the valproyl counterparts. Among various acyl functions examined, the relative potency was in the order of phenylbutyryl > phenylacetyl > butyryl > valproyl when conjugated to the same spacer and Zn^{2+}-chelating motif. Of these 12 derivatives, compound **19** was especially noteworthy. This hydroxamate-tethered phenylbutyrate (HTPB), i.e., compound **19**, exhibited an IC_{50} of 44 nM, a 4 order of magnitude improvement over phenylbutyrate. This optimal compound was used to examine its effect on HDAC activity in DU-145 prostate cancer cells.

Effect of HTPB on Histone Acetylation and $p21^{WAF/CIP1}$ Expression in DU-145 Prostate Cancer Cells. Histone hyperacetylation and increased expression of the cyclin-dependent kinase inhibitor $p21^{WAF/CIP1}$ represent two hallmark features in association with intracellular HDAC inhibition.[6] Consequently, we examined the effect of HTPB vis-à-vis TSA and phenylbutyrate on HDAC activity in DU-145 prostate cancer

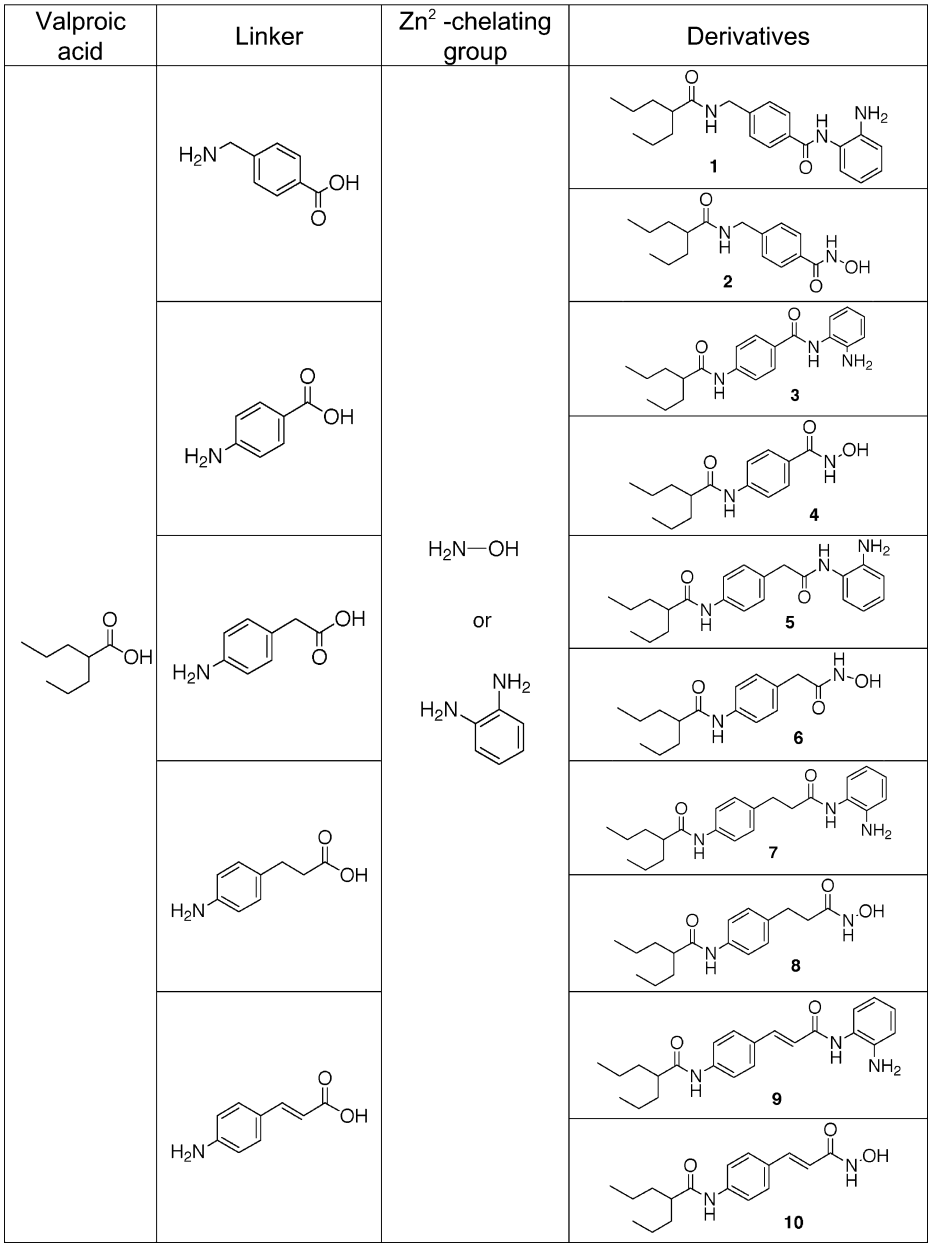

Figure 1. Divergent conjugations of valproic acid with five aromatic ω-amino acids and two Zn^{2+}-chelating moieties to generate compounds **1**−**10**.

cells by characterizing the status of histone acetylation and $p21^{WAF/CIP1}$ expression. DU-145 cells were exposed to HTPB at 0.5, 1, 2.5 μM, TSA at 0.25 and 0.5 μM, or phenylbutyrate at 1, 2.5, and 5 mM in 10% FBS-supplemented RPMI 1640 medium for 24 h. Western blot analysis of the cell lysates indicates that treatment of these agents gave rise to elevated levels of acetylated histones H3 and H4 and $p21^{WAF/CIP1}$ (Figure 4). The effect of 1 μM HTPB on these biomarkers approximated that of 0.25 μM TSA or 2.5 mM phenylbutyrate. DU-145 cells displayed small but significant amounts of intrinsic $p21^{WAF/CIP1}$, and the level increased substantially after exposure to HTPB as low as 0.5 μM. Together, these data confirmed that HTPB targeted HDAC activity in DU-145 cells.

Effect of HTPB on DU-145 Cell Viability. Effect of HTPB on cancer cell viability was assessed in DU-145 cells in 10% FBS-supplemented RPMI-1640 medium. These cells displayed a high degree of sensitivity to HTPB, with IC_{50} in growth inhibition of approximately between 0.5 and 1 μM (Figure 5A). As evidenced by DNA fragmentation, HTPB sensitized DU-145 cells to apoptosis in a dose-dependent manner (Figure 5B). As shown, extensive apoptosis occurred at 24 h when the drug concentration exceeded 1 μM, indicating that this cytotoxic effect was, at least in part, attributable to the induction of apoptosis by HDAC inhibition. Other cell lines examined including AN3CA endometrial cancer cells and SW-48 and HCT-15 colorectal cancer cells. These cancer cells were also susceptible to the cytotoxic effect of HTPB with similar potency (data not shown).

Discussion

In this paper, we report the development of a novel class of HDAC inhibitors, in which short-chain fatty acids were tethered to a Zn^{2+}-chelating moiety through hydrophobic linkage. This structural optimization was

Scheme 1[a]

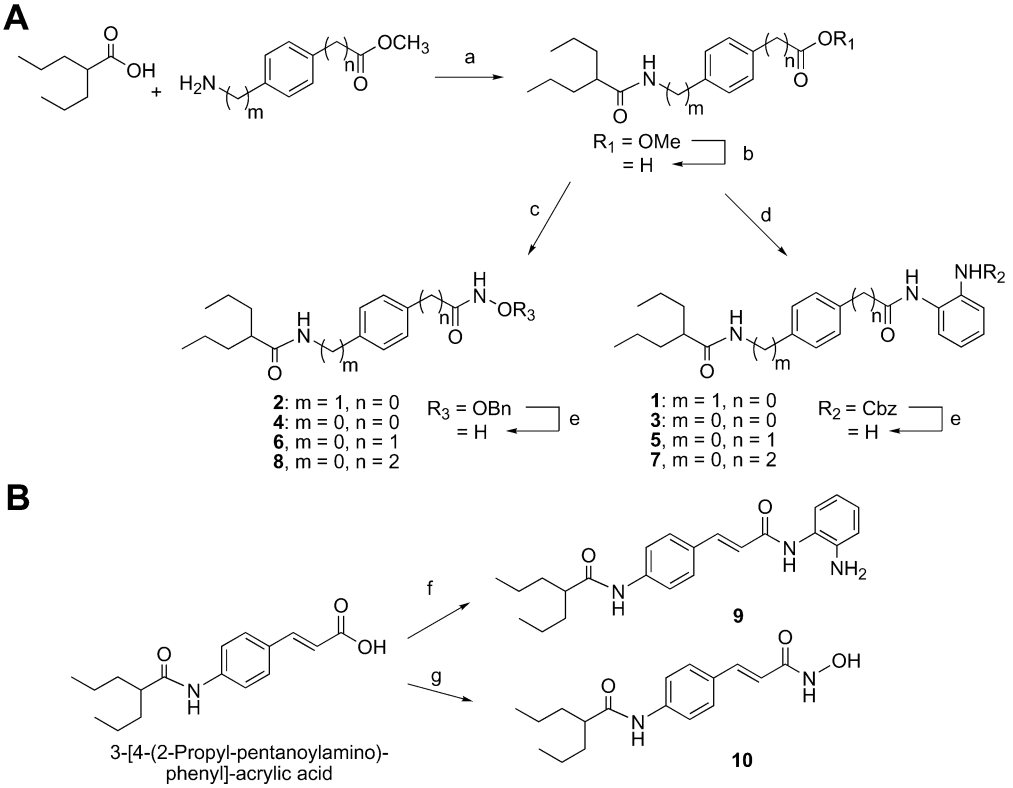

[a] Reagents: (a) EDC, THF; (b) KOH/MEOH, 80 °C; (c) NH_2OBn·HCl, BOPCl, Et_3N; (d) (2-aminopheny)carbamic acid benzyl ester, EDC, THF; (e) 10% PDC, H_2, MeOH/THF; (f) NH_2OH·HCl, EDC, HOBT, Et_3N; (g) *o*-phenylenediamine, EDC, THF.

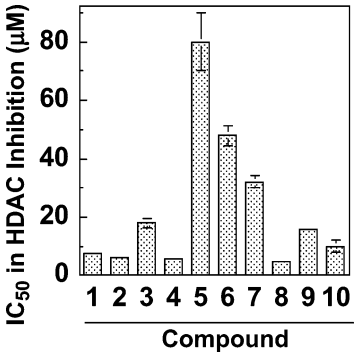

Figure 2. HDAC inhibitory potency of compounds **1**−**10**. In vitro HDAC assay was carried out by using a commercial enzyme assay kit as described in the Experimental Section. Data are the means ± SD (n = 3).

based on the working model provided by the unique mode of HDAC inhibition by TSA and SAHA.[27] This novel tethering strategy led to the discovery of HTPB (or compound **19**) that displays HDAC inhibitory and antiproliferative activities at submicromolar concentrations, which are in line with that reported for SAHA.[21] We obtained two lines of evidence that HTPB targeted HDAC activity in several cancer cell lines. Specifically, treatment of DU-145 prostate cancer cells with HTPB at as low as 0.5 μM caused the hyperacetylation of histones H-3 and H-4 in a dose-dependent manner. Likewise, $p21^{WAF/CIP1}$ expression was substantially upregulated in response to HTPB. In contrast, the parent molecule phenylbutyrate required at least 2.5 mM to achieve the same intracellular effects on histone acetylation and $p21^{WAF/CIP1}$ expression.

HTPB is structurally distinct from existing HDAC inhibitors, of which many have cap groups consisting of polar, planar structures. For example, the cap groups of TSA, SAHA, and MS-275 contain dimethylaminophenyl, phenylamino, and pyridin-3-yl-methoxycarbonyl groups, respectively. The present study suggests that the active-site pocket exhibited a high degree of flexibility in accommodating cap groups with different stereoelectronic properties. Our data indicate that phenylbutyryl and phenylacetyl were more effective than aliphatic acyl moieties in facilitating the binding of the conjugates to the active-site pocket. This discrepancy might, in part, be due to differences in electron density and/or steric hindrance imposed by the branched side chain. With regard to the aromatic linker, 4-aminobenzoate appeared to be optimal to tether phenylbutyryl with hydroxamate, of which the length was sufficient to make contacts at both ends of the pocket.

Conclusion

The efficacy of HTPB in HDAC inhibition demonstrates that potent HDAC inhibitors can be designed on the basis of the framework provided by the crystal structures of HDLP−ligand complexes. The present study presents a proof of principle that this tethering strategy allows the generation of a large library of compounds via the divergent combination of short-chain fatty acids, ω-amino acids, and hydroxamate. Further studies are under way to employ this strategy to develop HDAC isozyme-specific inhibitors.

Experimental Section

Chemical reagents and organic solvents were purchased from Aldrich unless otherwise mentioned. Nuclear magnetic

	R	Designation	IC_{50} (μM)
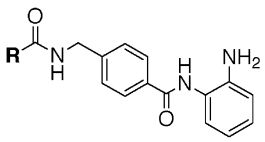	$CH_3CH_2CH_2$-	**11**	6.0 ± 0.5
		**12**	5.2 ± 0.4
	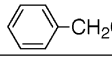	**13**	4.3 ± 0.3
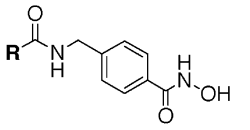	$CH_3CH_2CH_2$-	**14**	3.6 ± 0.5
		**15**	2.5 ± 0.3
	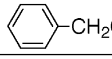	**16**	1.2 ± 0.1
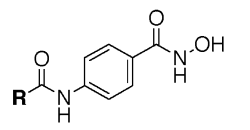	$CH_3CH_2CH_2$-	**17**	1.5 ± 0.2
		**18**	0.11 ± 0.01
	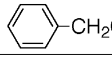	**19 (HTPB)**	0.044 ± 0.006
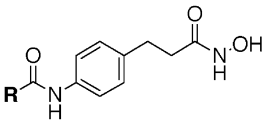	$CH_3CH_2CH_2$-	**20**	1.6 ± 0.2
		**21**	0.67 ± 0.08
	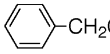	**22**	0.53 ± 0.06

Figure 3. Structures and HDAC inhibitory potency of compounds **11**−**22**. Values are the means ± SD ($n = 3$).

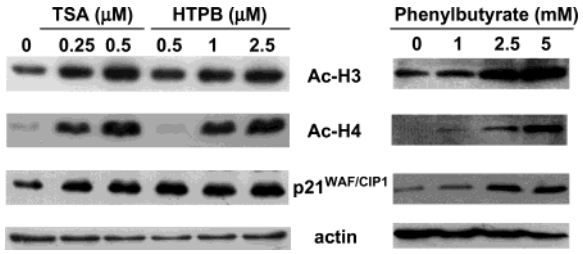

Figure 4. Effect of HTPB, TSA, and phenylbutyrate on histone acetylation and $p21^{WAF/CIP1}$ expression in DU-145 cells. DU-145 cells were exposed to HTPB, TSA, and phenylbutyrate at the indicated concentrations in 10% FBS-supplemented RPMI 1640 medium for 24 h. An equivalent amount of protein from individual lysates was electrophoresed and probed by Western blot with respective antibodies. Actin was used as an internal reference protein.

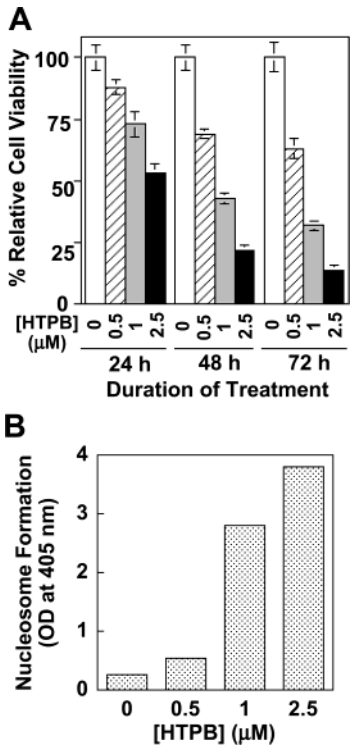

Figure 5. Growth inhibitory effect of HTPB on DU-145 cells. (A) Time course of the dose-dependent effect of HTPB on cell viability. DU-145 cells were treated with 0−2.5 μM HTPB in 10% FBS-containing RPMI 1640 medium for the indicated times. Viable cells were examined by the MTT assay. Data are means ± SD ($n = 6$). (B) Dose-dependent effect of HTPB on the formation of nucleosomal DNA after 24-h exposure. The formation of nucleosomes was quantitatively measured by cell death detection ELISA with lysates equivalent to 2×10^3 cells for each assay. Data are the average of two independent determinations.

resonance spectra (^{1}H NMR) were measured on Bruker 250 MHz. Chemical shifts (δ) are reported in parts per million (ppm) relative to TMS peak. Electrospray ionization (ESI) mass spectrometry analyses were performed with a 3-tesla Finnigan FTMS-2000 Fourier transform mass spectrometer. Elemental analyses were within ±0.4% of calculated values. Flash column chromatography was performed with silica gel (230−400 mesh). The ω-amino acid methyl esters were prepared from the commercially available acids using methanol/TMSCl, and (2-aminophenyl)carbamic acid benzyl ester was synthesized from *o*-phenylenediamine and benzyl chloride formate according to standard procedures. Rabbit anti-acetylhistone H3 and H4 polyclonal antibodies were purchased from Upstate Biotechnology (Lake Placid, NY), Rabbit anti-p21 antibodies were from Santa Cruz Biotechnology (Santa Cruz, CA). Mouse monoclonal anti-actin was from ICN Biomedicals.-(Irvine, CA). HRP-conjugated goat anti-rabbit IgG and HRP-conjugated goat anti-mouse IgG were from Jackson ImmunoResearch (West Grove, PA).

Compounds **1**−**8** and **11**−**22** were synthesized according to methods a−e described as follows (Scheme 1A), and compounds **9** and **10** were prepared from 3-[4-(2-propylpentanoylamino)-phenyl]acrylic acid by methods f and g, respectively (Scheme 1B), which are described separately under the title compounds.

Method a [1-(3-Dimethylaminopropyl)-3-ethylcarbodiimide Hydrochloride (EDC) Coupling]. To a solution of individual short-chain fatty acids in dry THF (5−10 mmol/mL) under N_2 was added various ω-amino acid methyl ester (1 equiv), followed by EDC (1.3 equiv). After stirring overnight, THF was removed under reduced pressure, and the residue was dissolved in ethyl acetate (100 mL). The mixture was washed consecutively with water (50 mL) twice and saturated

brine (50 mL). The organic layer was dried over Na_2SO_4 and concentrated under vacuum. The resulting residue was purified by silica gel flash chromatography.

Method b (Ester Cleavage). The resulting ester from method a was dissolved in a 2 M KOH/MeOH solution. The mixture was stirred at 80 °C for 1 h, cooled to 0 °C, acidified with 2 N HCl to pH 3, and concentrated under vacuum, and ethyl acetate (100 mL) and H_2O (50 mL) were added. The organic phase was separated, washed consecutively with water and saturated brine (50 mL each), dried over Na_2SO_4, and concentrated under vacuum. The resulting residue was purified by silica gel flash chromatography.

Method c [Bis(2-oxo-3-oxazolidinyl)phosphordiamidic Chloride (BOP−Cl) Coupling]. To a solution of the resulting acid from method b in dry THF (5−10 mmol/mL) was added triethylamine (TEA, 1 equiv) under N_2. The mixture was stirred at room temperature for 10 min, and BOP−Cl (1.1 equiv), *O*-benzylhydroxylamine hydrochloride (1 equiv), and TEA (3 equiv) were added. After stirring at room temperature overnight, the solution was concentrated under vacuum, and ethyl acetate (100 mL) was added, followed by 3% $NaHCO_3$ (50 mL). The organic phase was separated, washed consecutively with water and saturated brine (50 mL each), dried over Na_2SO_4, and concentrated under vacuum. The resulting residue was purified by silica gel flash chromatography.

Method d (EDC Coupling). To a solution of individual acids resulting from method b in dry THF (5−10 mmol/mL) under N_2 was added (2-aminophenyl)carbamic acid benzyl ester (1 equiv), followed by EDC (1.3 equiv). After stirring overnight, the mixture was concentrated under vacuum, and ethyl acetate (100 mL) was added. The organic phase was washed consecutively with water (50 mL) twice, followed by saturated brine (50 mL), dried over Na_2SO_4, and concentrated. The resulting residue was purified by silica gel flash chromatography.

Method e (Hydrogenolysis). The *N*-benzyloxy or *N*-Cbz derivative, resulting from method c or d, was dissolved in 1:1 methanol/THF (5−10 mmol/mL), and 10% palladium on charcoal (10% w/w) was added. The mixture was treated with hydrogen under atmospheric pressure for 2 h and filtered. The solvent was evaporated and the residue was recrystallized with ethyl acetate.

***N*-(2-Aminophenyl)-4-[(2-propylpentanoylamino)methyl]benzamide (1):** ^{1}H NMR (DMSO-d_6) δ 9.63 (s, 1 H), 8.45 (t, J = 6.1 Hz, 1 H), 7.94 (d, J = 7.8 Hz, 2 H), 7.36 (d, J = 8.3 Hz, 2 H), 7.16 (d, J = 7.6 Hz, 1 H), 6.98 (t, J = 7.5 Hz, 1 H), 6.78 (d, J = 7.7 Hz, 1 H), 6.60 (t, J = 7.6 Hz, 1 H), 4.90 (s, 2 H), 4.35 (d, J = 5.9 Hz, 2 H), 2.24 (m, 1 H), 1.6−1.1 (m, 8 H), 0.87 (t, 6 H); HRMS exact mass of $(M + Na)^+$, 390.215195 amu; observed mass of $(M + Na)^+$, 390.21793 amu. Anal. ($C_{22}H_{29}N_3O_2$) C, H, N.

***N*-Hydroxy-4-[(2-propylpentanoylamino)methyl]benzamide (2):** ^{1}H NMR (DMSO-d_6) δ 11.17 (s, 1 H), 9.00 (s, 1 H), 8.40 (t, J = 5.9 Hz, 1 H), 7.70 (d, J = 8.2 Hz, 2 H), 7 0.30 (d, J = 8.2 Hz, 2 H), 4.31 (d, J = 5.7 Hz, 2 H), 2.24 (m, 1 H), 1.6−1.1 (m, 8 H), 0.85 (t, 6 H); HRMS exact mass of $(M + Na)^+$, 315.167911 amu; observed mass of $(M + Na)^+$ 315.16755 amu. Anal. ($C_{16}H_{24}N_2O_3$) C, H, N.

***N*-(2-Aminophenyl)-4-(2-propylpentanoylamino)benzamide (3):** ^{1}H NMR (DMSO-d_6) δ 10.13 (s, 1 H), 9.57 (s, 1 H), 7.95 (d, J = 8.7 Hz, 2 H), 7 0.74 (d, J = 8.8 Hz, 2 H), 7.16 (d, J = 7.8 Hz, 1 H), 6.98 (t, J = 7.6 Hz, 1 H), 6.78 (d, J = 8.0 Hz, 1 H), 6.60 (t, J = 7.7 Hz, 1 H), 4.89 (s, 2 H), 2.44 (m, 1 H), 1.7−1.1 (m, 8 H), 0.89 (t, 6 H); HRMS exact mass of $(M + Na)^+$, 376.199545 amu; observed mass of $(M + Na)^+$, 376.19762 amu. Anal. ($C_{21}H_{27}N_3O_2$) C, H, N.

***N*-Hydroxy-4-(2-propylpentanoylamino)benzamide (4):** ^{1}H NMR (DMSO-d_6) δ 11.07 (s, 1 H), 10.13 (s, 1 H), 8.94 (s, 1 H), 7.65 (m, 4 H), 2.42 (m, 1 H), 1.7−1.1 (m, 8 H), 0.8 (t, 6 H); HRMS exact mass of $(M + Na)^+$, 301.152261 amu; observed mass of $(M + Na)^+$, 301.15194 amu. Anal. ($C_{15}H_{22}N_2O_3$) C, H, N.

2-Propylpentanoic acid {4-[(2-aminophenylcarbamoyl)-methyl]phenyl}amide (5): ^{1}H NMR (DMSO-d_6) δ 9.84 (s, 1 H), 9.33 (s, 1 H), 7.56 (d, J = 8.5 Hz, 2 H), 7.26 (d, J = 8.5 Hz, 2 H), 7.14 (d, J = 7.9 Hz, 1 H), 6.90 (t, J = 7.8 Hz, 1 H), 6.72 (d, J = 7.9 Hz, 1 H), 6.53 (t, J = 7.7 Hz, 1 H), 4.83 (s, 2 H), 2.41 (m, 1 H), 1.7−1.1 (m, 8 H), 0.89 (t, 6 H); HRMS exact mass of $(M + Na)^+$ 390.215195 amu; observed mass of $(M + Na)^+$, 390.21523 amu. Anal. ($C_{22}H_{29}N_3O_2$) C, H, N.

2-Propylpentanoic acid (4-hydroxyphenylcarbamoylmethylphenyl)amide (6): ^{1}H NMR (DMSO-d_6) δ 10.61 (s, 1 H), 9.82 (s, 1 H), 8.81 (s, 1 H), 7.52 (d, J = 8.5 Hz, 2 H), 7.16 (d, J = 8.5 Hz, 2 H), 3.22 (s, 2 H), 2.38 (m, 1 H), 1.7−1.1 (m, 8 H), 0.89 (t, 6 H); HRMS exact mass of $(M + Na)^+$, 315.167911 amu; observed mass of $(M + Na)^+$, 315.16751 amu. Anal. ($C_{16}H_{24}N_2O_3$) C, H, N.

2-Propylpentanoic acid {4-[2-(2-amino-phenylcarbamoyl)-ethyl]phenyl}amide (7): ^{1}H NMR (DMSO-d_6) δ 9.80 (s, 1 H), 9.15 (s, 1 H), 7.53 (d, J = 8.4 Hz, 2 H), 7.17 (d, J = 8.4 Hz, 2 H), 7.11 (d, J = 7.8 Hz, 1 H), 6.89 (t, J = 7.9 Hz, 1 H), 6.70 (d, J = 7.9 Hz, 1 H), 6.53 (t, J = 7.7 Hz, 1 H), 4.80 (s, 2 H), 2.86 (t, J = 7.9 Hz, 2 H), 2.59 (t, J = 8.1 Hz, 2 H), 2.38 (m, 1 H), 1.7−1.1 (m, 8 H), 0.87 (t, 6 H); HRMS exact mass of $(M + Na)^+$, 404.230845 amu; observed mass of $(M + Na)^+$ 404.23043 amu. Anal. ($C_{23}H_{31}N_3O_2$) C, H, N.

2-Propylpentanoic acid [4-(2-hydroxyphenylcarbamoyl)ethyl)phenyl]amide (8): ^{1}H NMR (DMSO-d_6) δ 10.38 (s, 1 H), 9.78 (s, 1 H), 8.70 (s, 1 H), 7.50 (d, J = 8.5 Hz, 2 H), 7.10 (d, J = 8.5 Hz, 2 H), 2.75 (t, J = 7.3 Hz, 2 H), 2.40 (m, 1 H), 2.22 (t, J = 7.4 Hz, 2 H), 1.7−1.1 (m, 8 H), 0.87 (t, 6 H); HRMS exact mass of $(M + Na)^+$, 329.183561 amu; observed mass of $(M + Na)^+$ 329.18295 amu. Anal. ($C_{17}H_{26}N_2O_3$) C, H, N.

3-[4-(2-Propylpentanoyl)phenyl]acrylic Acid. This compound, a precursor to compounds **9** and **10**, was synthesized from 2-propylpentanoic acid (0.78 mL, 4.9 mmol) and 3-(4-aminophenyl)acrylic acid methyl ester (0.86 g, 4.9 mmol) according to methods a and b aforementioned: total yield, 1.05 g (70% for two steps); ^{1}H NMR ($CDCl_3$, 10% DMSO-d_6) δ 9.49 (s, 1 H), 7.71 (d, J = 8.5 Hz, 2 H), 7.55 (d, J = 15.9 Hz, 1 H), 7.45 (d, J = 8.4 Hz, 2 H), 6.31 (d, J = 15.9 Hz, 1 H), 2.40 (m, 1 H), 1.7−1.1 (m, 8 H), 0.87 (t, 6 H).

***N*-(2-Aminophenyl)-3-[4-(2-propylpentanoylamino)phenyl]acrylamide (9).** To a solution of 3-[4-(2-propylpentanoyl)-phenyl]acrylic acid (200 mg, 0.7 mmol) in dry THF was added benzene-1,2-diamine (450 mg, 4.2 mmol) under N_2, followed by EDC (180 mg, 0.9 mmol). After stirring overnight, the mixture was concentrated under vacuum, ethyl acetate (50 mL) was added, and the reaction mixture was washed consecutively with water (30 mL) twice and saturated brine (30 mL). The organic layer was dried over Na_2SO_4 and concentrated under vacuum. The crude product was purified by flash chromatography (ethyl acetate−hexane, 1:1), giving compound **9** (200 mg, 76% yield) as white solid: ^{1}H NMR (DMSO-d_6) δ 10.07 (s, 1 H), 9.35 (s, 1 H), 7.71 (d, J = 8.6 Hz, 2 H), 7.56 (d, J = 8.5 Hz, 2 H), 7.51 (d, J = 15.7 Hz, 1 H), 7.34 (d, J = 6.6 Hz, 1 H), 6.92 (t, J = 7.1 Hz, 1 H), 6.80 (d, J = 15.5 Hz, 1 H), 6.75 (d, J = 6.6 Hz, 1 H), 6.58 (t, J = 7.3 Hz, 1 H), 4.96 (s, 2 H), 2.44 (m, 1 H), 1.7−1.1 (m, 8 H), 0.87 (t, 6 H); HRMS exact mass of $(M + Na)^+$, 402.215195 amu; observed mass of $(M + Na)^+$, 402.21448 amu. Anal. ($C_{23}H_{29}N_3O_2$) C, H, N.

***N*-Hydroxy-3-[4-(2-propylpentanoylamino)phenyl]acrylamide (10).** To a solution of 3-[4-(2-propylpentanoylamino)-phenyl]acrylic acid (100 mg, 0.35 mmol) in dry DMF (3 mL) was added EDC (79 mg, 0.53 mmol) and hydroxybenzotriazole hydrate (HOBT) (62 mg, 0.46 mmol) under nitrogen. The mixture was stirred for 1 h, and hydroxylamine hydrochloride (27.4 mg, 0.39 mmol) and TEA (54 μL) were added. The mixture was stirred for an additional 12 h and concentrated under vacuum, and ethyl acetate (40 mL) and saturated $NaHCO_3$ solution (15 mL) were added. The organic phase was separated and washed consecutively with water and saturated brine (20 mL each). The organic layer was dried over Na_2SO_4 and concentrated under vacuum. The crude product was purified by flash chromatography [ethyl acetate−MeOH (9:1)], yielding compound **10** (45 mg, 40% yield) as white solid: ^{1}H NMR (DMSO-d_6) δ 10.69 (s, 1 H), 10.07 (s, 1 H), 9.00 (s, 1

H), 7.67 (d, $J = 7.9$ Hz, 2 H), 7.53 (d, $J = 8.4$ Hz, 2 H), 7.39 (d, $J = 15.6$ Hz, 1 H), 6.39 (d, $J = 15.3$ Hz, 1 H), 2.40 (m, 1 H), 1.7−1.1 (m, 8 H), 0.87 (t, 6 H); HRMS exact mass of $(M + Na)^+$, 327.167911 amu; observed mass of $(M + Na)^+$, 327.16809 amu. Anal. ($C_{17}H_{24}N_2O_3$) C, H, N.

***N*-(2-Aminophenyl)-4-(butyrylaminomethyl)benzamide (11):** ^{1}H NMR (DMSO-d_6) δ 9.63 (s, 1 H), 8.41 (t, $J = 5.7$ Hz, 1 H), 7.94 (d, $J = 8.1$ Hz, 2 H), 7 0.36 (d, $J = 8.0$ Hz, 2 H), 7.17 (d, $J = 7.6$ Hz, 1 H), 6.98 (t, $J = 7.6$ Hz, 1 H), 6.78 (d, $J = 8.1$ Hz, 1 H), 6.60 (t, $J = 7.7$ Hz, 1 H), 4.90 (s, 2 H), 4.35 (d, $J = 5.8$ Hz, 2 H), 2.15 (t, $J = 7.3$ Hz, 2 H), 1.60 (m, 2 H), 0.88 (t, $J = 7.3$ Hz, 3 H); HRMS exact mass of $(M + Na)^+$, 334.152595 amu; observed mass of $(M + Na)^+$, 334.15221 amu. Anal. ($C_{18}H_{21}N_3O_2$) C, H, N.

***N*-(2-Aminophenyl)-4-(phenylacetylaminomethyl)benzamide (12):** ^{1}H NMR (DMSO-d_6) δ 9.60 (s, 1 H), 8.66 (t, $J = 6.1$ Hz, 1 H), 7.92 (d, $J = 8.2$ Hz, 2 H), 7 0.31 (m, 7 H), 7.16 (d, $J = 7.0$ Hz, 1 H), 6.98 (t, $J = 7.4$ Hz, 1 H), 6.78 (d, $J = 6.6$ Hz, 1 H), 6.60 (t, $J = 7.4$ Hz, 1 H), 4.90 (s, 2 H), 4.35 (d, $J = 5.7$ Hz, 2 H), 3.51 (s, 2 H); HRMS exact mass of $(M + Na)^+$, 382.152595 amu; observed mass of $(M + Na)^+$, 382.15228 amu. Anal. ($C_{22}H_{21}N_3O_2$) C, H, N.

***N*-(2-Aminophenyl)-4-[(4-phenylbutyrylamino)methyl]benzamide (13):** ^{1}H NMR (DMSO-d_6) δ 9.63 (s, 1 H), 8.43 (t, $J = 6.1$ Hz, 1 H), 7.94 (d, $J = 8.3$ Hz, 2 H), 7.34 (d, $J = 8.3$ Hz, 2 H), 7 0.21 (m, 6 H), 6.98 (t, $J = 7.2$ Hz, 1 H), 6.78 (d, $J = 8.11$ Hz, 2 H), 6.61 (t, $J = 6.5$ Hz, 1 H), 4.90 (s, 2 H), 4.34 (d, $J = 6.1$ Hz, 2 H), 2.59 (t, $J = 7.6$ Hz, 2 H), 2.20 (t, $J = 7.7$ Hz, 2 H), 1.84 (m, 2 H); HRMS exact mass of $(M + Na)^+$, 410.183895 amu; observed mass of $(M + Na)^+$, 410.18232 amu. Anal. ($C_{24}H_{25}N_3O_2$) C, H, N.

4-(Butyrylaminomethyl)-*N*-hydroxybenzamide (14): ^{1}H NMR (DMSO-d_6) δ 11.15 (s, 1 H), 9.01 (s, 1 H), 8.36 (t, $J = 5.6$ Hz, 1 H), 7.7 (d, $J = 8.1$ Hz, 2 H), 7 0.32 (d, $J = 8.0$ Hz, 2 H), 4.30 (d, $J = 5.7$ Hz, 2 H), 2.15 (t, $J = 7.3$ Hz, 2 H), 1.60 (m, 2 H), 0.88 (t, $J = 7.3$ Hz, 3 H); HRMS exact mass of $(M + Na)^+$, 259.10569 amu; observed mass of $(M + Na)^+$, 259.10569 amu. Anal. ($C_{12}H_{16}N_2O_3$) C, H, N.

***N*-Hydroxy-4-(phenylacetylaminomethyl)benzamide (15):** ^{1}H NMR (DMSO-d_6) δ 11.2 (s, 1 H), 8.9 (s, 1 H), 8.6 (t, $J = 5.8$ Hz, 1 H), 7.9 (d, $J = 8.3$ Hz, 2 H), 7.28 (m, 7 H), 4.04 (d, $J = 5.7$ Hz, 2 H), 3.5 (s, 2 H); HRMS exact mass of $(M + Na)^+$, 307.105311 amu; observed mass of $(M + Na)^+$, 307.10512 amu. Anal. ($C_{16}H_{16}N_2O_3$) C, H, N.

***N*-Hydroxy-4-[(4-phenylbutyrylamino)methyl]benzamide (16):** ^{1}H NMR (DMSO-d_6) δ 11.2 (s, 1 H), 9.0 (s, 1 H), 8.4 (t, $J = 5.8$ Hz, 1 H), 7.7 (d, $J = 8.0$ Hz, 2 H), 7.21 (m, 7 H), 4.3 (d, $J = 5.8$ Hz, 2 H), 2.58 (t, $J = 7.3$ Hz, 2 H), 2.18 (t, $J = 7.3$ Hz, 2 H), 1.83 (m, 2 H); HRMS exact mass of $(M + Na)^+$, 335.136611 amu; observed mass of $(M + Na)^+$, 335.13716 amu. Anal. ($C_{18}H_{20}N_2O_3$) C, H, N.

4-Butyrylamino-*N*-hydroxybenzamide (17): ^{1}H NMR (DMSO-d_6) δ 11.08 (s, 1 H), 10.09(s, 1 H), 8.94 (s, 1 H), 7.67 (m, 4 H), 2.31 (t, $J = 7.3$ Hz, 2 H), 1.61 (m, 2 H), 0.92 (t, $J = 7.4$ Hz, 3 H); HRMS exact mass of $(M + Na)^+$, 245.089661 amu; observed mass of $(M + Na)^+$, 245.08971 amu; difference <1.0 ppm. Anal. ($C_{11}H_{14}N_2O_3$) C, H, N.

***N*-Hydroxy-4-phenylacetylaminobenzamide (18):** ^{1}H NMR (DMSO-d_6) δ 11.1 (s, 1 H), 10.40 (s, 1 H), 8.94 (s, 1 H), 7.67 (m, 4 H), 7.33 (m, 5 H), 3.67 (s, 2 H); HRMS exact mass of $(M + Na)^+$, 293.089661 amu; observed mass of $(M + Na)^+$, 293.08957 amu. Anal. ($C_{15}H_{14}N_2O_3$) C, H, N.

***N*-Hydroxy-4-(4-phenylbutyrylamino)benzamide (19):** ^{1}H NMR (DMSO-d_6) δ 11.02 (s, 1 H), 10.1 (s, 1 H), 8.94 (s, 1 H), 7.67 (m, 4 H), 7.27 (m, 5 H), 2.63 (t, $J = 7.5$ Hz, 2 H), 2.35 (t, $J = 7.4$ Hz, 2 H), 1.87 (m, 2 H); HRMS exact mass of $(M + Na)^+$, 321.120961 amu; observed mass of $(M + Na)^+$, 321.11940 amu. Anal. ($C_{17}H_{18}N_2O_3$) C, H, N.

***N*-[4-(2-Hydroxycarbamoylethyl)phenyl]butyramide (20):** ^{1}H NMR (DMSO-d_6) δ 10.4 (s, 1 H), 9.8 (s, 1 H), 8.70 (s, 1 H), 7.50 (d, $J = 8.4$ Hz, 2 H), 7.10 (d, $J = 8.4$ Hz, 2 H), 2.75 (t, $J = 7.3$ Hz, 2 H), 2.24 (m, 4 H), 1.61 (m, 2 H), 0.92 (t, $J = 7.4$ Hz, 3 H); HRMS exact mass of $(M + Na)^+$, 273.120961 amu; observed mass of $(M + Na)^+$, 273.12080 amu. Anal. ($C_{13}H_{18}N_2O_3$) C, H, N.

***N*-Hydroxy-3-(4-phenylacetylaminophenyl)propionamide (21):** ^{1}H NMR (DMSO-d_6) δ 10.36 (s, 1 H), 10.14 (s, 1 H), 8.70 (s, 1 H), 7.50 (d, $J = 8.3$ Hz, 2 H), 7.2−7.4 (m, 5 H), 7.10 (d, $J = 8.3$ Hz, 2 H), 3.62 (s, 2 H), 2.75 (t, $J = 7.5$ Hz, 2 H), 2.22 (t, $J = 7.6$ Hz, 2 H); HRMS exact mass of $(M + Na)^+$ 321.120961 amu; observed mass of $(M + Na)^+$, 321.12040 amu. Anal. ($C_{17}H_{18}N_2O_3$) C, H, N.

***N*-[4-(2-Hydroxycarbamoylethyl)phenyl]-4-phenylbutyramide (22):** ^{1}H NMR (DMSO-d_6) δ 10.36 (s, 1 H), 9.80 (s, 1 H), 8.70 (s, 1 H), 7.52 (d, $J = 8.5$ Hz, 2 H), 7.2−7.4 (m, 5 H), 7.10 (d, $J = 8.4$ Hz, 2 H), 2.75 (t, $J = 7.4$ Hz, 2 H), 2.62 (t, $J = 7.5$ Hz, 2 H), 2.15−2.4 (m, 4 H), 1.8−2.0 (m, 2 H); HRMS exact mass of $(M + Na)^+$, 349.152261 amu; observed mass of $(M + Na)^+$, 349.15223 amu. Anal. ($C_{19}H_{22}N_2O_3$) C, H, N.

In Vitro HDAC Assay. HDAC activity was analyzed by using a histone deacetylase assay kit (Upstate Biotechnology, Lake Placid, NY) by following the manufacturer's instruction with slight modifications. This assay was based on the ability of DU-145 nuclear extract, which is rich in histone deacetylase activity, to mediate the deacetylation of biotinylated [^{3}H]acetyl histone H4 peptide that was bound to streptavidin agarose beads. The release of [^{3}H]acetate into the supernatant was measured to calculate the HDAC activity. Sodium butyrate (0.25−1 mM) was used as a positive control.

Cell Viability Assay. The effect of HTPB on cell viability was assessed by the MTT {[3-(4,5-dimethylthiazol-2-yl)-2,5-diphenyl-2*H*-tetrazolium bromide]} assay in 96-well, flat-bottomed plates, in which 4000 DU-145 cells/well were seeded. Cells were exposed to HTPB at the indicated concentrations in 10% FBS-supplemented RPMI-1640 medium at 37 °C in 5% CO_2 for the indicated time. The medium was removed and replaced by 150 μL of 0.5 mg/mL of MTT in RPMI-1640 medium, and cells were incubated in the CO_2 incubator at 37 °C for 2 h. Supernatants were removed from the wells, and the reduced MTT dye was solubilized with 200 μL/well DMSO. Absorbance was determined on a plate reader at 570 nm. Each treatment was repeated in six wells.

Apoptosis Detection by An Enzyme-Linked Immunosorbent Assay (ELISA). Induction of apoptosis was assessed by using a cell death detection ELISA (Roche Diagnostics, Mannheim, Germany) by following the manufacturer's instruction. This test is based on the quantitative determination of cytoplasmic histone-associated DNA fragments in the form of mononucleosomes and oligonucleosomes after induced apoptotic death. In brief, 1×10^6 DU-145 cells were cultured in a T-75 flask 24 h prior to the experiment. Cells were treated with HTPB at the indicated concentrations in 10% FBS-supplemented RPMI 1640 medium. Both floating and adherent cells were collected, and cell lysates equivalent to 2×10^3 cells were used in the ELISA.

Western Blot Analysis. DU-145 cells (1×10^6) treated with HTPB at the indicated concentrations in 10% FBS-supplemented RPMI 1640 medium for 24 h were collected and sonicated. Protein concentrations of the lysates were determined by using a Bradford protein assay kit (Bio-Rad, Hercules, CA); equivalent amounts of proteins from each lysate were resolved in 10% SDS−polyacrylamide gel and then transferred onto Immobilon-nitrocellulose membranes (Millipore, Bellerica, MA) in a semidry transfer cell. The transblotted membrane was washed twice with Tris-buffered saline (TBS) containing 0.1% Tween 20 (TBST). After blocking with TBST containing 5% nonfat milk for 40 min, the membrane was incubated with the primary antibody (1:1000 dilution) in TBST−1% nonfat milk at 4 °C overnight. After treatment with the primary antibody, the membrane was washed three times with TBST for a total of 15 min, followed by goat anti-rabbit or anti-mouse IgG-horseradish peroxidase conjugates (diluted 1:3000) for 1 h at room temperature and wash three times with TBST for a total of 1 h. The immunoblots were visualized by enhanced chemiluminescence.

Acknowledgment. This investigation was supported by Army Grant DAMD17-02-1-0117 and National Institutes of Health Grant CA94829 (to C.-S.C.).

Note Added after ASAP Posting. This manuscript was released ASAP on 12/11/2003 with commas that should not be present in the title. The correct version was posted on 12/22/2003.

References

(1) Kouzarides, T. Histone acetylases and deacetylases in cell proliferation. *Curr. Opin. Genet. Dev.* **1999**, *9*, 40−48.
(2) Gray, S. G.; Ekstrom, T. J. The human histone deacetylase family. *Exp. Cell Res.* **2001**, *262*, 75−83.
(3) Jenuwein, T.; Allis, C. D. Translating the histone code. *Science* **2001**, *293*, 1074−1080.
(4) Wade, P. A. Transcriptional control at regulatory checkpoints by histone deacetylases: Molecular connections between cancer and chromatin. *Hum. Mol. Genet.* **2001**, *10*, 693−698.
(5) Cress, W. D.; Seto, E. Histone deacetylases, transcriptional control, and cancer. *J. Cell Physiol.* **2000**, *184*, 1−16.
(6) Marks, P.; Rifkind, R. A.; Richon, V. M.; Breslow, R.; Miller, T.; et al. Histone deacetylases and cancer: Causes and therapies. *Nat. Rev. Cancer* **2001**, *1*, 194−202.
(7) Jung, M. Inhibitors of histone deacetylase as new anticancer agents. *Curr. Med. Chem.* **2001**, *8*, 1505−1511.
(8) Grozinger, C. M.; Schreiber, S. L. Deacetylase enzymes: Biological functions and the use of small-molecule inhibitors. *Chem. Biol.* **2002**, *9*, 3−16.
(9) Johnstone, R. W. Histone-deacetylase inhibitors: Novel drugs for the treatment of cancer. *Nat. Rev. Drug Discov.* **2002**, *1*, 287−299.
(10) Kramer, O. H.; Gottlicher, M.; Heinzel, T. Histone deacetylase as a therapeutic target. *Trends Endocrinol. Metab.* **2001**, *12*, 294−300.
(11) Marks, P. A.; Richon, V. M.; Rifkind, R. A. Histone deacetylase inhibitors: Inducers of differentiation or apoptosis of transformed cells. *J. Natl. Cancer Inst.* **2000**, *92*, 1210−1216.
(12) Lea, M. A.; Tulsyan, N. Discordant effects of butyrate analogues on erythroleukemia cell proliferation, differentiation and histone deacetylase. *Anticancer Res.* **1995**, *15*, 879−883.
(13) Kruh, J. Effects of sodium butyrate, a new pharmacological agent, on cells in culture. *Mol. Cell Biochem.* **1982**, *42*, 65−82.
(14) Newmark, H. L.; Young, C. W. Butyrate and phenylacetate as differentiating agents: Practical problems and opportunities. *J. Cell Biochem. Suppl.* **1995**, *22*, 247−253.
(15) Phiel, C. J.; Zhang, F.; Huang, E. Y.; Guenther, M. G.; Lazar, M. A.; et al. Histone deacetylase is a direct target of valproic acid, a potent anticonvulsant, mood stabilizer, and teratogen. *J. Biol. Chem.* **2001**, *276*, 36734−36741.
(16) Suzuki, T.; Ando, T.; Tsuchiya, K.; Fukazawa, N.; Saito, A.; et al. Synthesis and histone deacetylase inhibitory activity of new benzamide derivatives. *J. Med. Chem.* **1999**, *42*, 3001−3003.
(17) Saito, A.; Yamashita, T.; Mariko, Y.; Nosaka, Y.; Tsuchiya, K.; et al. A synthetic inhibitor of histone deacetylase, MS-27-275, with marked in vivo antitumor activity against human tumors. *Proc. Natl. Acad. Sci. U.S.A.* **1999**, *96*, 4592−4597.
(18) Tsuji, N.; Kobayashi, M.; Nagashima, K.; Wakisaka, Y.; Koizumi, K. A new antifungal antibiotic, trichostatin. *J. Antibiot. (Tokyo)* **1976**, *29*, 1−6.
(19) Jung, M.; Brosch, G.; Kolle, D.; Scherf, H.; Gerhauser, C.; et al. Amide analogues of trichostatin A as inhibitors of histone deacetylase and inducers of terminal cell differentiation. *J. Med. Chem.* **1999**, *42*, 4669−4679.
(20) Furumai, R.; Komatsu, Y.; Nishino, N.; Khochbin, S.; Yoshida, M.; et al. Potent histone deacetylase inhibitors built from trichostatin A and cyclic tetrapeptide antibiotics including trapoxin. *Proc. Natl. Acad. Sci. U.S.A.* **2001**, *98*, 87−92.
(21) Richon, V. M.; Emiliani, S.; Verdin, E.; Webb, Y.; Breslow, R.; et al. A class of hybrid polar inducers of transformed cell differentiation inhibits histone deacetylases. *Proc. Natl. Acad. Sci. U.S.A.* **1998**, *95*, 3003−3007.
(22) Remiszewski, S. W.; Sambucetti, L. C.; Atadja, P.; Bair, K. W.; Cornell, W. D.; et al. Inhibitors of human histone deacetylase: Synthesis and enzyme and cellular activity of straight chain hydroxamates. *J. Med. Chem.* **2002**, *45*, 753−757.
(23) Kijima, M.; Yoshida, M.; Sugita, K.; Horinouchi, S.; Beppu, T. Trapoxin, an antitumor cyclic tetrapeptide, is an irreversible inhibitor of mammalian histone deacetylase. *J. Biol. Chem.* **1993**, *268*, 22429−22435.
(24) Shute, R. E.; Dunlap, B.; Rich, D. H. Analogues of the cytostatic and antimitogenic agents chlamydocin and HC-toxin: Synthesis and biological activity of chloromethyl ketone and diazomethyl ketone functionalized cyclic tetrapeptides. *J. Med. Chem.* **1987**, *30*, 71−78.
(25) Han, J. W.; Ahn, S. H.; Park, S. H.; Wang, S. Y.; Bae, G. U.; et al. Apicidin, a histone deacetylase inhibitor, inhibits proliferation of tumor cells via induction of p21WAF1/Cip1 and gelsolin. *Cancer Res.* **2000**, *60*, 6068−6074.
(26) Nakajima, H.; Kim, Y. B.; Terano, H.; Yoshida, M.; Horinouchi, S. FR901228, a potent antitumor antibiotic, is a novel histone deacetylase inhibitor. *Exp. Cell Res.* **1998**, *241*, 126−133.
(27) Finnin, M. S.; Donigian, J. R.; Cohen, A.; Richon, V. M.; Rifkind, R. A.; et al. Structures of a histone deacetylase homologue bound to the TSA and SAHA inhibitors. *Nature* **1999**, *401*, 188−193.
(28) Sternson, S. M.; Wong, J. C.; Grozinger, C. M.; Schreiber, S. L. Synthesis of 7200 small molecules based on a substructural analysis of the histone deacetylase inhibitors trichostatin and trapoxin. *Org. Lett.* **2001**, *3*, 4239−4242.

JM0303655